

The relaxed eddy accumulation method over the Amazon forest: the importance of flux strength on individual and aggregated flux estimates.

Nelson Luís Dias (✉ nldias@ufpr.br)

Federal University of Paraná

Ivan Mauricio Cely Toro

Federal Institute of Pará

Cléo Quaresma Dias-Júnior

Federal Institute of Pará

Luca Mortarini

Institute of Atmospheric Sciences and Climate

Daiane Brondani

University of Urbino

Research Article

Keywords: Roughness sublayer, ATTO project, REA method

Posted Date: June 27th, 2023

DOI: <https://doi.org/10.21203/rs.3.rs-3092504/v1>

License:   This work is licensed under a Creative Commons Attribution 4.0 International License.

[Read Full License](#)

Additional Declarations: No competing interests reported.

Version of Record: A version of this preprint was published at Boundary-Layer Meteorology on October 4th, 2023. See the published version at <https://doi.org/10.1007/s10546-023-00829-7>.

1 **The relaxed eddy acumulation method over the**
2 **Amazon forest: the importance of flux strength on**
3 **individual and aggregated flux estimates.**

4 **Nelson Luís Dias · Ivan Mauricio Cely**
5 **Toro · Cléo Quaresma Dias-Júnior ·**
6 **Luca Mortarini · Daiane Brondani**

7
8 Received: DD Month YEAR / Accepted: DD Month YEAR

9 **Abstract**

10 The ability of the Relaxed Eddy Accumulation (REA) method to estimate the
11 kinematic fluxes of temperature, water vapor and carbon dioxide was assessed
12 for the dry season (3 months) at the ATTO (Amazon Tall Tower Observatory)
13 site from turbulence measurements. The measurements were performed at 50
14 m above ground within the roughness sublayer. Non-conformity with inertial
15 sublayer conditions was confirmed one more time by analyzing dimensionless
16 scalar standard deviations. Recently found results that the REA method out-
17 performs Monin-Obukhov-based approaches are confirmed. Over the scale of
18 the whole dry season, REA and EC (eddy covariance) estimates are essen-
19 tially equal. However, we also verify that such results fail to reveal significant
20 variability and scatter of the REA estimates when the fluxes are of small mag-
21 nitude. On the basis of previous studies, we conjecture that this is caused by a
22 likely imbalance between scalar gradient production and molecular dissipation.

N. L. Dias

Department of Environmental Engineering, Federal University of Paraná, Brazil.
E-mail: nldias@ufpr.br

I. M. C. Toro

Department of Physics, Federal Institute of Pará, Belém, Brazil
E-mail: mauriciocelytoro@gmail.com

C. Q. Dias-Jr

Department of Physics, Federal Institute of Pará, Belém, Brazil
E-mail: cleo.quaresma@ifpa.edu.br

L. Mortarini

Department of Physics, Universidade Federal de Santa Maria, RS, Brazil and Institute of
Atmospheric Sciences and Climate, National Research Council (ISAC-CNR), Torino, Italy
E-mail: l.mortarini@isac.cnr.it

D. Brondani

Department of Pure and Applied Sciences (DiSPeA), University of Urbino “Carlo Bo”, Italy
E-mail: meteorologia.daia@gmail.com

Confirmation of our results to trace gases, therefore, requires further study.

Keywords Roughness sublayer, ATTO project, REA method

1 Introduction

The Relaxed Eddy Accumulation (REA) method, proposed by Businger and Oncley (1990), is a simplification of the Eddy Accumulation Method conceived by R. L. Desjardins (1972; 1977). The most important feature of the REA method from the experimental point of view is that it does not require a fast-response instrument to measure the scalar concentration s whose turbulent flux is wanted. Instead, the sign of the vertical velocity w is used in real time to switch a valve drawing air at a constant flow rate into two different reservoirs. At the end of a block of measurement, the mean concentration of the scalar can be measured by a slow-response sensor in each of the reservoirs. In this work, note that the REA method is actually simulated using fast-response sensors.

The REA method has gained wide use to measure surface fluxes of substances for which fast-response gas analyzers are either non-existent or impractical. In that capacity, it has been reported to measure isoprene (Bowling et al. 1998), ammonia (Zhu et al. 2000), terpenoid (Mochizuki et al. 2014) and ethene, propene, buthene and isoprene (Rhew et al. 2017) fluxes, to cite but a few.

The REA predicts the scalar turbulent flux from

$$\overline{w's'} = \beta_s \sigma_w (\overline{s^+} - \overline{s^-}), \quad (1)$$

where $\overline{s^+} = \overline{[s|w > 0]}$ and $\overline{s^-} = \overline{[s|w < 0]}$ are the conditional means of s on the sign of the vertical velocity w (under the assumption that $\overline{w} = 0$, so that $w = w'$), and the overbars and primes are standard notation for Reynolds' decomposition into a mean and the fluctuation around it. In the present work all means are taken over 30-minute blocks. For conciseness, we denote $\overline{s^+} - \overline{s^-}$ by $\Delta\overline{s}$.

From its inception, it has been recognized that under validity of Monin-Obukhov Similarity Theory (MOST), β_s should be a function of Obukhov's stability variable ζ (Businger and Oncley 1990); several studies have found $\beta_s \approx 0.6$ with a modest variation of $\approx 10\%$ over a wide range of stabilities when the measurements are made in the inertial sublayer of the atmospheric surface layer (see, for example, Businger and Oncley 1990; Baker et al. 1992; Katul et al. 2018).

Over forests, an important issue is to estimate the fluxes from the canopy to the atmosphere of Volatile Organic Compounds (VOCs) such as isoprene; this is particularly critical in the Amazon, where secondary organic aerosols have a significant role in the formation of cloud condensation nuclei (CCNs) (Fuentes et al. 2016). Here, due to the aforementioned difficulty of measuring VOC

63 concentrations with fast-response instruments, the REA method can have a
64 significant impact on closing the knowledge gap on VOC emission rates from
65 the forest. It is also noteworthy that new, better and cheaper technologies for
66 *in-situ* analysis of $\Delta\bar{s}$ are emerging that leverage the applicability of the REA
67 method (Sarkar et al. 2020).

68 Invariably, REA measurements require a sonic anemometer measuring w
69 at high frequency to control in real time the valve switching the flow of air into
70 two reservoirs for the measurement of $\overline{s^+}$ and $\overline{s^-}$ at the end of a measurement
71 block. This means that simultaneous measurements of sonic temperature θ are
72 available, allowing standard eddy covariance (EC) measurements of $\overline{w'\theta'}$. This
73 in turn means that, for each block, β_θ can be calculated from (1) with $s = \theta$.
74 Therefore, if the scalar s of interest is perfectly correlated to temperature, β_s
75 may be allowed to vary from block to block by setting $\beta_s = \beta_\theta$ for each block.
76 This strategy, which we call “REA-T”(where “T” stands for auxiliary sonic
77 temperature measurements) appears to have originated with Bowling et al.
78 (1998), and is in wide use (Ren et al. 2011; Mochizuki et al. 2014; Rhew et al.
79 2017; Sarkar et al. 2020, etc.). Alternatively, of course, one can still adopt a
80 single value of β_s (which we call “REA-S”, where “S” stands for “single value”)
81 based on measurements of s with eddy covariance (using instrumentation with
82 adequate response time) or again an assumption of similar behavior with more
83 easily measured quantities.

84 Either way, the REA invokes (i) an assumption of similarity between scalars,
85 or (ii) the validity of MOST for the scalar of interest or (iii) at least the con-
86 stancy of β_s even if MOST does not apply. Strictly speaking, it is known that
87 if MOST is valid for any pair of scalars, their similarity functions must be
88 the same, and their correlation must be perfect (Hill 1989; Dias and Brutsaert
89 1996; Dias 2013). Most of the time, therefore, either (i) or (ii) seems to be
90 warranted for measurements made in the inertial sublayer of the atmospheric
91 boundary layer, where MOST is assumed to hold over homogeneous surfaces
92 with sufficient fetch.

93 However, even under these conditions, recently evidence has emerged that
94 MOST may not be universally valid for *all* scalars, but rather that it appears
95 to depend on the equilibrium between gradient production and dissipation of
96 scalar semivariance: the presence of relatively large values of other terms in
97 the scalar semivariance budget, such as the storage or the transport terms,
98 can seriously disrupt MOST conformity for the scalar in question (Zahn et al.
99 2023). Interestingly, in the same study Zahn et al. (2023) have found that
100 the REA method is much superior to the variance method (a classical MOST
101 indirect method to estimate scalar fluxes) even when equilibrium between
102 gradient production and molecular dissipation does not hold for the scalar,
103 which suggests that in this case (iii) may be valid at least on average.

104 In the roughness sublayer (RSL) over a forest there is strong evidence
105 of large departures of scalar behavior from MOST (Dias et al. 2009; Zahn
106 et al. 2016b; Chor et al. 2017). Zahn et al. (2016b) found large departures for
107 all 3 scalars (temperature, H₂O and CO₂) measured at the ATTO (Amazon
108 Tall Tower Observatory) site in Central Amazonia (see description below),

109 but noted that scalar similarity improved significantly for small zenith angles.
 110 They also found considerable scatter in the β_s values, which again was reduced
 111 for small zenith angles, which happen in the middle of the day, when the scalar
 112 fluxes tend to be largest in absolute value. In order to be concise, in this work
 113 we call fluxes which are large in absolute value “large-magnitude” fluxes.

114 Chor et al. (2017) equally found strong dissimilar behavior for the same
 115 scalars, as well as wide scatter in their Monin-Obukhov integral similarity
 116 functions. This casts doubt on the applicability of the REA method in any of
 117 the two forms (β_s constant or $\beta_s = \beta_\theta$ for each block) mentioned above, while
 118 at the same time is at odds with the recent findings of Zahn et al. (2023) of
 119 good REA performance, although the latter were obtained for a lake, not a
 120 forest.

121 Using a large dataset recently measured at the ATTO site, this work there-
 122 fore has the objective to clarify some of the issues mentioned above, and in
 123 particular to answer the following questions:

- 124 1. How close to constant is β_s (*i.e.* what its typical scatter is), and to what ex-
 125 tent do the REA-related stability functions follow MOST in the roughness
 126 sublayer?
- 127 2. How good are block-by-block REA flux estimates in the Amazonian rough-
 128 ness sublayer?
- 129 3. How good is the REA for “long-term” (of the order of many days to a
 130 whole season), “mean” flux estimates?

131 The relevant relationships among the quantities of interest in this work are
 132 reviewed in Section 2; the ATTO site and details of data processing are given
 133 in Section 3; results for similarity functions are analyzed in Section 4, and for
 134 the actual prediction of fluxes in Section 5. Discussion and conclusions are
 135 given in Section 6.

136 2 Methods

137 Since the “variance method” has shown to be a good indicator of the break-
 138 down of MOST in the RSL (Dias et al. 2009; Zahn et al. 2016b; Chor et al.
 139 2017; Dias-Júnior et al. 2019), and even in a classical inertial sublayer (Zahn
 140 et al. 2023), we test its standard form

$$\frac{\sigma_s}{s_*} = \phi_{\sigma_s}(\zeta), \quad (2)$$

141 with

$$u_*^2 = -\overline{u'w'}, \quad (3)$$

$$\zeta = -\frac{\kappa g(z - d_0)\theta_*}{\overline{\theta}u_*^2}, \quad (4)$$

$$u_*s_* = \overline{w's'}, \quad (5)$$

$$\sigma_s = \sqrt{\overline{s's'}}, \quad (6)$$

142 where u is the longitudinal velocity, z is the measurement height, and d_0 is
 143 the zero-plane displacement height.

144 In the case of the REA method, it can be readily seen by rearranging (1)
 145 that (see Zahn et al. 2023, Eq. (17))

$$\frac{1}{\beta_s} = \frac{\sigma_w \Delta \bar{s}}{w' s'} = \frac{\sigma_w}{u_*} \frac{\Delta \bar{s}}{s_*} = \phi_{\sigma_w}(\zeta) \phi_{\Delta \bar{s}}(\zeta). \quad (7)$$

146 where $\sigma_w/u_* = \phi_{\sigma_w}(\zeta)$ and $\Delta \bar{s}/s_* = \phi_{\Delta \bar{s}}(\zeta)$, and that β_s is an MOST function
 147 under ideal conditions.

148 Regarding (1), (2) and (7), two points are concerned:

- 149 1. Experimentally, “to be or not to be” a function of ζ is largely a matter of
 150 assessing the goodness-of-fit of data to a proposed model. Although this is
 151 seldom —if at all— done in practice for MOST functions (to the best of
 152 our knowledge), it is possible to quantify such goodness-of-fit by standard
 153 statistical indices. Therefore, in this study we compare quantitatively ϕ_{σ_w} ,
 154 ϕ_{σ_s} and $\phi_{\Delta \bar{s}}$ as described in the sequence.
- 155 2. As we will see in Section 4, the quality of the $\phi(\zeta)$ s or even the variability of
 156 β_s do not translate directly to the quality of the estimated fluxes $\overline{w' s'}$ over
 157 different time scales (block-by-block or longer term). Therefore, a second
 158 quantitative assessment must be made of the quality of the estimated fluxes
 159 themselves.

160 Besides graphical comparisons, we compare predicted (y) to observed (x)
 161 values using standard statistics: coefficient of correlation r , coefficient of de-
 162 termination C_d , BIAS, mean absolute error MAE, root mean square error
 163 RMSE, their normalized versions NBIAS, NMAE, NRMSE, and Willmott’s
 164 refined index of model performance d_r (Willmott et al. 2012). An important
 165 issue here is that small magnitudes of predicted and observed fluxes tend to
 166 be masked both graphically in traditional “ $x \times y$ ” plots and statistically when
 167 directly quantified, say, by RMSE or MAE. For this reason, the normalized
 168 versions are better to discern “relative” errors. For the sake of completeness,
 169 these quantities are

$$r = \frac{\text{Cov}(x, y)}{\sigma_x \sigma_y}, \quad C_d = 1 - \frac{\text{MSE}}{\sigma_x^2}, \quad (8)$$

$$\text{BIAS} = \frac{1}{n} \sum_{i=1}^n (y_i - x_i), \quad \text{NBIAS} = \frac{\text{BIAS}}{|\bar{x}|}, \quad (9)$$

$$\text{MAE} = \frac{1}{n} \sum_{i=1}^n |y_i - x_i|, \quad \text{NMAE} = \frac{\text{MAE}}{|\bar{x}|}, \quad (10)$$

$$\text{RMSE} = \left[\frac{1}{n} \sum_{i=1}^n (y_i - x_i)^2 \right]^{1/2}, \quad \text{NRMSE} = \frac{\text{RMSE}}{|\bar{x}|}. \quad (11)$$

170 where $\text{Cov}(x, y)$ is the covariance between predicted and observed values, σ_x
 171 and σ_y are their standard deviations, \bar{x} is the mean of the observed values,

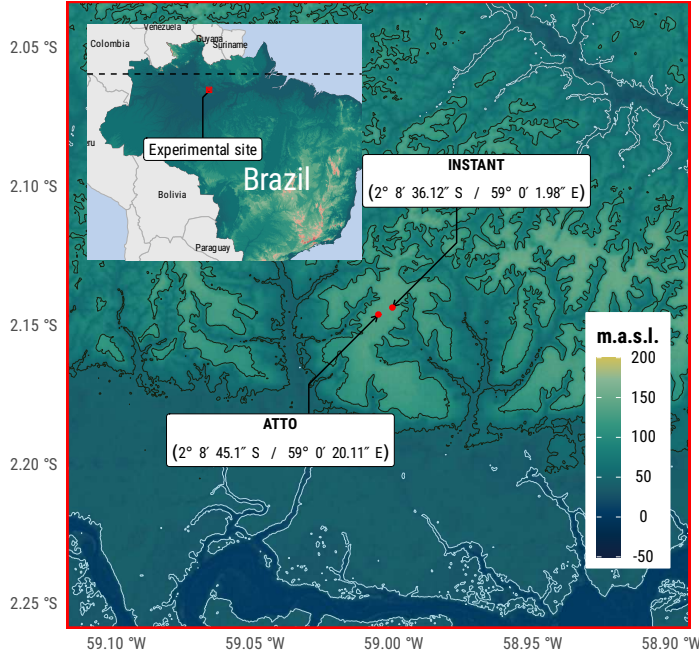


Fig. 1 Overall location of the ATTO site.

172 and $MSE = RMSE^2$ is the mean square error. Note that if all predicted values
 173 are equal, r makes no sense because $\sigma_y = 0$. Willmott's refined index of
 174 performance is

$$d_r = \begin{cases} 1 - \frac{\sum_{i=1}^n |y_i - x_i|}{2 \sum_{i=1}^n |x_i - \bar{x}|}, & \sum_{i=1}^n |y_i - x_i| \leq 2 \sum_{i=1}^n |x_i - \bar{x}|, \\ \frac{2 \sum_{i=1}^n |x_i - \bar{x}|}{\sum_{i=1}^n |y_i - x_i|} - 1, & \sum_{i=1}^n |y_i - x_i| > 2 \sum_{i=1}^n |x_i - \bar{x}|. \end{cases} \quad (12)$$

175 3 Experimental site and data

176 In this work we used data collected at a micrometeorological tower built up
 177 at the experimental ATTO (Amazon Tall Tower Observatory) site, in Central
 178 Amazon, in a *terra firme* forest, approximately 150 km northeast from the city
 179 of Manaus — AM, Brazil. At the site, there are two towers that are situated
 180 on an extensive plateau area (130 m above sea level) immersed in a large
 181 primary forest (see Figure 1). The vegetation is typical of undisturbed *terra*
 182 *firme* forest. The average height of the vegetation is approximately 30 to 40
 183 m and the leaf area index is around 5 to 6 $m^2 m^{-2}$. The predominant wind is
 184 from the northeast (Andreae et al. 2015; Santana et al. 2018).

185 There are two towers at the ATTO site, known as the (main) ATTO tower
 186 ($02^\circ 08' 45'' S$, $59^\circ 00' 20'' W$) with a height of 325 m and the “Instant” tower

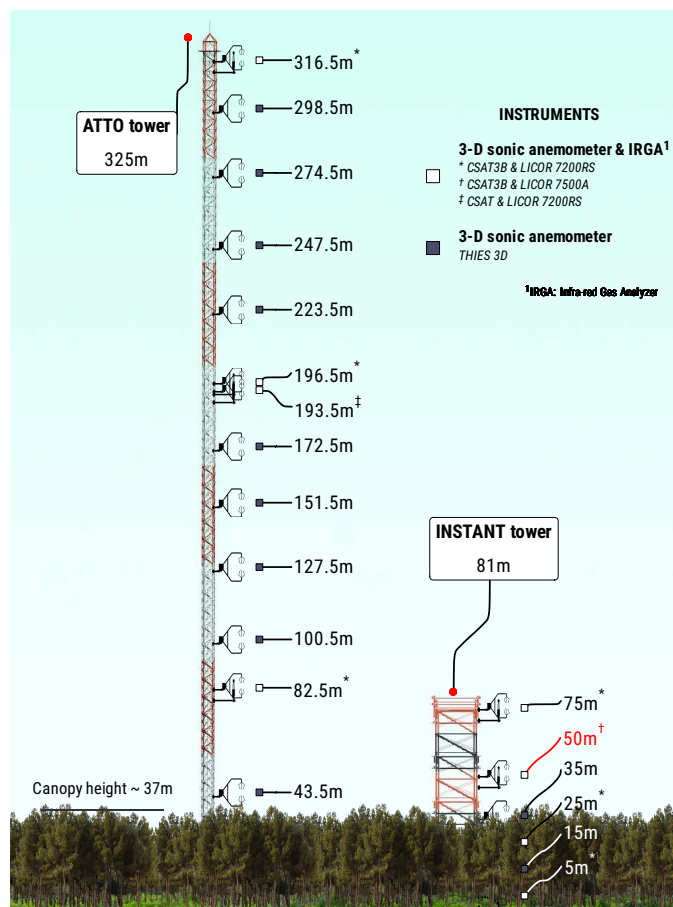


Fig. 2 Instrument setup of the ATTO site. In this work, only the 50-m data from the Instant Tower were used.

187 (02° 08' 39" S, 59° 00' 00" W) with a height of 81 m (Dias-Júnior et al. 2019).
 188 The experimental setup is shown in Figure 2. The experimental data used
 189 in this work were collected during the months of August, September, and
 190 October 2021. These months correspond to the dry season in the Amazon
 191 region. The data were measured at 10 Hz by a sonic anemometer (model
 192 CSAT3B, Campbell Scientific, Inc) and an open-path gas analyzer (model
 193 LICOR 7500A LI-COR Inc), both installed 50 m above the ground at the
 194 Instant tower.

195 The dataset was divided in 3959 30-minute data blocks. A quality control
 196 analysis similar to the one described in Zahn et al. (2016a) was applied to
 197 u , v , w (velocity components of the sonic anemometer), θ (sonic temperature),
 198 ω_q (H_2O molar density) and ω_c (CO_2 molar density) for each block. The
 199 procedure divides a block with n data points ($n = 18000$ in our case) into $n_s =$
 200 n/m sub-blocks with m points each. One-minute sub-blocks, $m = 600$, were

used. Before quality control, missing or erroneous data were flagged as NaNs; then, for each sub-block, the median \tilde{x}_k and the mean absolute deviation (MAD_k) around it,

$$\text{MAD}_k = \frac{1}{m} \sum_{i=0}^{m-1} |x_{km+i} - \tilde{x}_k| \quad (13)$$

were evaluated. The sub-block index, k , runs from 0 to $n_s - 1$. For each sub-block:

- A spike is identified each time $|x_{km+i} - \tilde{x}_k| > 5 \text{ MAD}_k$;
- a locking condition (i.e. x_i varies too little over a sub-block) is identified if $\max_k(\text{MAD}_k) < 0.01$ (K for θ , m s^{-1} for u , v and w and mmol m^{-3} for ω_q and ω_c);
- a non-stationary condition is identified if the difference between the maximum and minimum sub-block medians is larger than Q_x , where $Q_{u,v} = 5 \text{ m s}^{-1}$, $Q_w = 3 \text{ m s}^{-1}$, $Q_\theta = 5 \text{ K}$, $Q_{\omega_q} = 300 \text{ mmol m}^{-3}$ and $Q_{\omega_c} = 10 \text{ mmol m}^{-3}$.

When all the above conditions were met, the following criteria were applied sequentially:

1. If the number of values equal to NaN in the block was more than 1% of the block size, all x_i were set to NaN and the block was effectively discarded;
2. All spikes were flagged as NaN. After that, if the number of values equal to NaN in the block was more than 1% of the block size, all x_i were set to NaN and the block was effectively discarded;
3. If a locking condition and/or a non-stationary condition were identified, all the half-hour block was set to NaN and again discarded from the analysis;
4. If the block was not discarded, all runs of NaNs in x were linearly interpolated from the valid extremities.

After conducting the quality control analysis, we obtained 1146 blocks of 30 minutes each for ω_c , 1163 blocks for ω_q , 1307 blocks for θ , u , v , and w . In addition, we computed the half-hourly mean values of turbulence statistics by applying two coordinate rotations (McMillen 1988) to ensure that the average lateral and vertical velocities were zero. For all subsequent analyses the H_2O and CO_2 molar densities ω_q and ω_c were converted to instantaneous mass concentrations using the pressure sensor from the LI7500 (see for instance Edson et al. 2011). In this work they are reported as q in g kg^{-1} and c in mg kg^{-1} respectively. Note that covariances calculated with mass concentrations dispense with the WPL density corrections (Webb et al. 1980).

4 Results for similarity functions

4.1 Similarity functions for the classical standard deviation statistics

Standard inertial sublayer (ISL) predictions for ϕ_{σ_w} and ϕ_{σ_s} are (Chor et al. 2017)

$$\phi_{\sigma_w}(\zeta) = \begin{cases} 1.25(1 - 3\zeta)^{1/3}, & \zeta < 0, \\ 1.25, & \zeta \geq 0, \end{cases} \quad (14)$$

$$\phi_{\sigma_s}(\zeta) = \begin{cases} 2(1 - 9.5\zeta)^{-1/3}, & \zeta < 0, \\ 2, & \zeta \geq 0. \end{cases} \quad (15)$$

When calculating the statistics σ_s/s_* , we further filtered the data with sign restrictions for each scalar and stability condition. Thus, in the case of θ , we only use $\Delta\bar{\theta} < 0$ for stable conditions ($\theta_* < 0$) and $\Delta\bar{\theta} > 0$ for unstable conditions ($\theta_* > 0$); for q , we only use positive values of $\overline{w'q'}$ and only positive values of both $\Delta\bar{q}$ and q_* for both stable and unstable conditions; and in the case of c we only use $\Delta\bar{c} > 0$ for stable conditions, with $c_* > 0$, and $\Delta\bar{c} < 0$ for unstable conditions, with $c_* < 0$. The further restrictions on the signs of $\Delta\bar{s}$ were imposed so that exactly the same data sets were used for both similarity functions ϕ_{σ_s} and $\phi_{\Delta\bar{s}}$, and therefore corresponding statistics and figures can be compared. After the flux comparisons of Section 5 were computed, 3 more blocks (08/08/2021 2045UTC, 18/08/2021 2015UTC and 19/09/2021 2245UTC) produced very pronounced outliers when plotted that biased all statistics considerably. Therefore, these blocks were not included in any of the statistics or figures shown in this work.

Figure 3 shows the statistics σ_w/u_* , and σ_s/s_* for $s = \theta$, $s = q$ and $s = c$ for stable and unstable conditions, respectively. The findings of Zahn et al. (2016b) and Chor et al. (2017) for the ATTO site (but generally valid for the roughness sublayer over forests) are confirmed: overall, there is an excess of scalar variance in comparison to flux (actually s_*), giving strong indication that gradient production of $\overline{s's'}/2$ often is far less than scalar molecular dissipation (see Zahn et al. 2023); however, a detailed analysis of the semivariance scalar budgets falls outside of our scope. The σ_w/u_* statistics are somewhat less “well-behaved” than those obtained by Zahn et al. (2016b) and Chor et al. (2017) for the same site: under unstable conditions, there is a clear tendency for many blocks to display *less* variance in comparison to flux (actually u_*), suggesting that now a part of the gradient and buoyant production of TKE (turbulence kinetic energy) is being “exported” rather than dissipated locally. This is indicative of a negative transport of TKE in the RSL above the canopy (see Fig. 1b of Chamecki et al. 2020 and Mortarini et al. 2023).

Besides the standard ISL versions of $\phi_\sigma(\zeta)$ shown in blue, we also obtained least-squares (using the Levenberg-Marquardt algorithm) estimates depicted

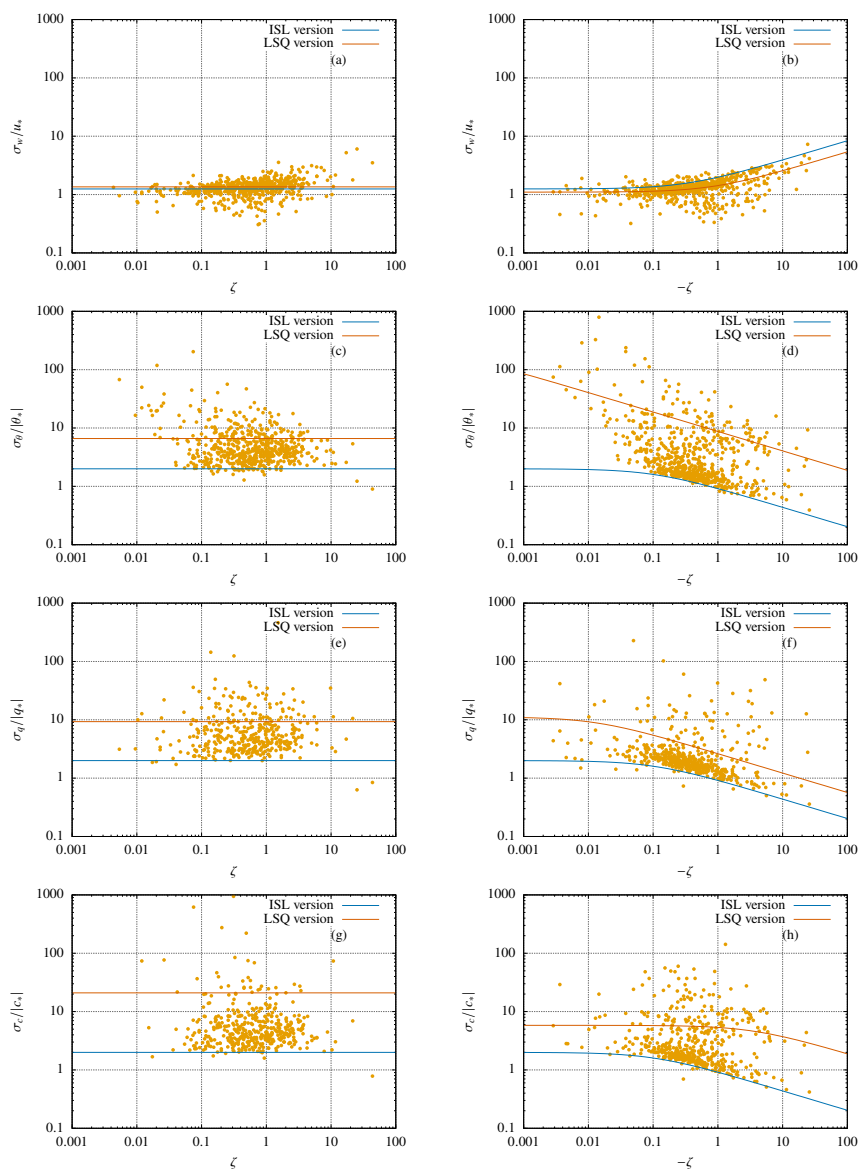


Fig. 3 Dimensionless values of σ_w/u_* (a,b) and σ_s/s_* for $s = \theta$ (c,d), $s = q$ (e,f) and $s = c$ (g,h), for stable (a,c,e,g) and unstable (b,d,f,h) conditions. The blue line is the standard inertial sublayer (ISL) prediction and the vermilion line is a least-squares (LSQ) fit.

Table 1 Least-squares estimates of coefficients for $\phi_{\sigma_w}(\zeta)$ and $\phi_{\sigma_s}(\zeta)$ for $s = \theta, q, c$.

Variable	a	b	c
w	1.10166	1.16819	1.35627
θ	198.159	11677.3	6.61057
q	11.1756	76.3461	9.31149
c	5.81312	0.281669	20.9179

Table 2 Performance statistics for the LSQ functions $\phi_{\sigma_w}(\zeta)$ and $\phi_{\sigma_s}(\zeta)$ for $s = \theta, q, c$. For stable conditions, the ϕ_{σ_s} are constant and r cannot be calculated.

Variable	r	C_d	BIAS	MAE	RMSE	d_r
Stable conditions						
w	—	-0.0005	-0.0136	0.3257	0.5965	0.5025
θ	—	-0.0017	-4.7637	9.2032	116.1735	0.6308
q	—	0.0000	0.0196	7.4759	25.5693	0.4993
c	—	0.0000	0.0458	28.7931	185.0199	0.4993
Unstable conditions						
w	0.6266	0.3918	0.0035	0.2721	0.4146	0.5922
θ	0.3802	0.0905	4.1461	12.7000	37.3868	0.4089
q	0.1075	0.0108	-0.1343	3.6464	12.2686	0.5075
c	0.0480	0.0023	0.0039	4.9986	10.0795	0.4982

270 in vermilion in Figure 3 with the general forms

$$\phi_{\sigma_w}(\zeta) = a_w(1 - b_w\zeta)^{1/3}, \quad \zeta < 0, \quad (16)$$

$$\phi_{\sigma_w}(\zeta) = c_w, \quad \zeta \geq 0, \quad (17)$$

$$\phi_{\sigma_s}(\zeta) = a_s(1 - b_s\zeta)^{-1/3}, \quad \zeta < 0, \quad (18)$$

$$\phi_{\sigma_s}(\zeta) = c_s, \quad \zeta \geq 0. \quad (19)$$

271 The values of the fitted coefficients are given in Table 1. As it can be seen both
 272 visually and from the coefficients in the table, the fitted (LSQ) versions differ
 273 significantly from their ISL counterparts, but by definition they still provide
 274 the “best fits”. Note that the large excursions of a relatively small percentage
 275 of points can have a significant impact on the estimates of a , b and c .

276 Table 2 shows the performance statistics obtained for the LSQ versions
 277 (not the ILS versions) of the similarity functions ϕ_{σ_w} and ϕ_{σ_s} . Note that these
 278 functions are all dimensionless, so there is no need to calculate normalized
 279 performance statistics. The statistics confirm the visual impression that, par-
 280 ticularly for the scalars, the dimensionless standard deviations perform rather
 281 poorly, with generally small correlations between data points and predicted
 282 ϕ_{σ_s} s, and large values of MAE and RSME (for dimensionless functions, a
 283 good outcome would be MAE, RMSE ~ 0.1).

Table 3 Least-squares estimates of coefficients for $\phi_{\Delta\bar{s}}(\zeta)$ for $s = \theta, q, c$.

Variable	a	b	c
θ	11.0134	696.671	1.41662
q	1.77719	1.86711	1.46055
c	1.68725	0.198108	1.59865

Table 4 Performance statistics for the LSQ functions $\phi_{\Delta\bar{s}}(\zeta)$ for $s = \theta, q, c$. For stable conditions, the ϕ_{σ_s} s are constant and r cannot be calculated.

Variable	r	C_d	BIAS	MAE	RMSE	d_r
Stable conditions						
θ	—	-0.0017	-0.2611	0.8132	6.3909	0.5677
q	—	0.0000	0.0025	0.5882	0.9941	0.4993
c	—	0.0000	0.0019	0.7763	2.4383	0.4994
Unstable conditions						
θ	0.3237	0.1011	-0.0653	1.0226	2.3101	0.4938
q	0.3007	0.0894	-0.0038	0.3517	0.7250	0.5640
c	0.1235	0.0148	0.0022	0.5990	1.0200	0.4994

284 4.2 Similarity functions for the REA statistics

285 Figure 4 shows the statistics of $\Delta\bar{s}/s_*$ and the similarity functions $\phi_{\Delta\bar{s}}(\zeta)$
 286 fitted by least squares. The same general form of (18)–(19) was used:

$$\phi_{\Delta\bar{s}}(\zeta) = a_{\Delta\bar{s}}(1 - b_{\Delta\bar{s}}\zeta)^{-1/3}, \quad \zeta < 0, \quad (20)$$

$$\phi_{\Delta\bar{s}}(\zeta) = c_{\Delta\bar{s}}, \quad \zeta \geq 0. \quad (21)$$

287 The corresponding values are shown in Table 3.

288 Because these functions have only been explicitly proposed very recently
 289 by Zahn et al. (2023), these may be the first results obtained in a roughness
 290 sublayer over a forest. Visually, the $\phi_{\Delta\bar{s}}$ values are significantly less scattered
 291 than their ϕ_{σ_s} counterparts, indicating that REA dimensionless statistics may
 292 be potentially more useful than standard deviation ones. This is confirmed
 293 quantitatively in Table 4, where MAE and RMSE for the $\phi_{\Delta\bar{s}}$ s are at least
 294 an order of magnitude less than the corresponding values in Table 2. Clearly,
 295 the REA dimensionless statistics behave better (as a “function” of ζ) in the
 296 roughness sublayer than their dimensionless standard deviation counterparts:
 297 a physical explanation for this is not at hand and will require further research.
 298 However, the scatter is still relatively large and this is probably a consequence
 299 of measurements made within the RSL.

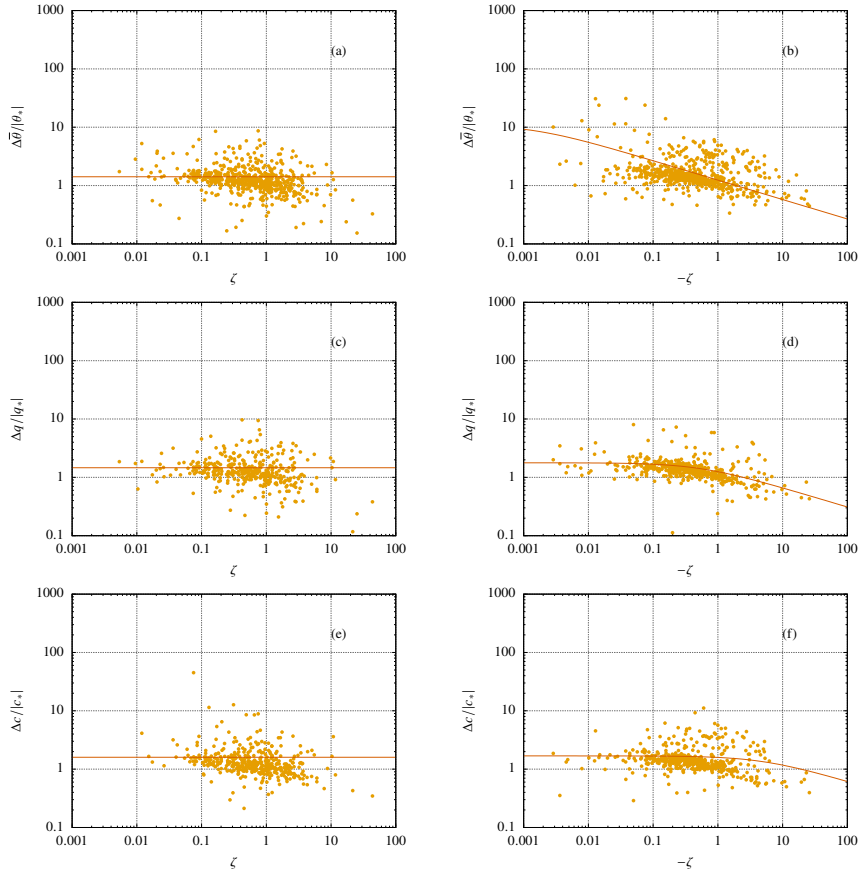


Fig. 4 Dimensionless values of $\Delta\bar{s}/s_*$ for $s = \theta$ (a,b), $s = q$ (c,d) and $s = c$ (e,f) for stable (a,c,e) and unstable (b,d,f) conditions. The vermilion line is a least-squares (LSQ) fit.

300 5 Results for predicted fluxes

301 5.1 Flux estimates from dimensionless standard deviations (variance method)

302 When MOST does not apply for a particular scalar s , it makes little sense to
 303 estimate its turbulent fluxes from the standard deviation similarity function
 304 $\phi_{\sigma_s}(\zeta)$, given the unacceptable scatter seen in Figure 3 and the corresponding
 305 performance statistics in Table 2. Here, we re-do this exercise not because it is
 306 applicable in practice for our site, but because (a) it highlights the role of large
 307 magnitude fluxes on visual and numerical evaluation of the results; and (b) it
 308 provides a baseline to assess the gains in applying the REA method, as done
 309 by Zahn et al. (2023). We estimate the fluxes $\overline{w's'}$ using the observed values
 310 of u_* ; an iterative procedure is performed for $s = \theta$ by starting at $\zeta = 0$ and

Table 5 Performance statistics for the kinematic fluxes $\overline{w'\theta'}$ ($\text{m s}^{-1}\text{K}$), $\overline{w'q'}$ ($\text{m s}^{-1} \text{g kg}^{-1}$), $\overline{w'c'}$ ($\text{m s}^{-1} \text{mg kg}^{-1}$), estimated by the variance method. BIAS, MAE and RMSE are given in the same corresponding units.

Variable	r	C_d	BIAS	NBIAS	MAE	NMAE	RMSE	NRMSE	d_r
Stable conditions									
$\overline{w'\theta'}$	0.8625	0.6151	0.0037	0.3641	0.0051	0.5000	0.0093	0.9103	0.6624
$\overline{w'q'}$	0.8171	0.4899	-0.0040	-0.4894	0.0048	0.5803	0.0132	1.6138	0.6900
$\overline{w'c'}$	0.6660	-0.0662	-0.1218	-0.7701	0.1259	0.7957	0.2035	1.2865	0.4862
Unstable conditions									
$\overline{w'\theta'}$	0.3913	-0.7875	-0.0558	-0.9257	0.0564	0.9351	0.0816	1.3532	0.4526
$\overline{w'q'}$	0.7911	-0.7318	-0.0610	-0.7600	0.0625	0.7786	0.0799	0.9961	0.3797
$\overline{w'c'}$	0.5136	-0.3213	0.2791	0.5975	0.3217	0.6888	0.4237	0.9072	0.4676

311 calculating θ_* (from Eq. (2)) and ζ (from Eq. (4)) until convergence in θ_* ; and
312 then q_* and c_* are obtained again from Eqs. (2) and (4). All kinematic fluxes
313 are then obtained from Eq. (5). Note that we are using the whole dataset both
314 for estimating the coefficients a , b and c in (18)–(19) and for evaluating the
315 performance of the estimated fluxes, since our intention here is only to assess
316 the *relative* merits of the variance and REA methods.

317 Figure 5 shows the kinematic fluxes predicted by the variance method. For θ
318 under unstable conditions, the predicted fluxes are much smaller in magnitude
319 than the observed ones. This means that $\zeta \approx 0$ always for the prediction of
320 the other two fluxes. In spite of that, we see that there is always a linear trend
321 (and often a large linear correlation) between observed and predicted values.
322 The corresponding performance statistics are given in Table 5. The very large
323 magnitude of the errors is clearly discernible by the (large) values of NBIAS,
324 NMAE and NRMSE.

325 The spread of the small fluxes is difficult to discern in Figure 5. To empha-
326 size the *relative* error made in flux estimation, we re-plot the same results in
327 Figure 6. Now we plot the ratios of predicted to observed fluxes in the vertical
328 axes, against the observed fluxes in the horizontal axes. The blue lines are the
329 medians of the ratios. The figure shows how the large magnitude fluxes tend
330 to have a small spread around the median, but that the spread of the small
331 magnitude fluxes is exceptionally large: we are truncating the vertical axes at
332 a maximum value of 10, but larger ratios do occur in the dataset. Clearly, if we
333 restrict the conditions so that only larger flux values are probed, the variance
334 method will tend to perform better in the RSL: this is very likely what hap-
335 pened for small zenith angles in Zahn et al. (2016b). The physical mechanism
336 explaining this is probably that, for large-magnitude fluxes, gradient produc-
337 tion of scalar semivariance will be strong enough to balance, approximately,
338 molecular dissipation of scalar variance.

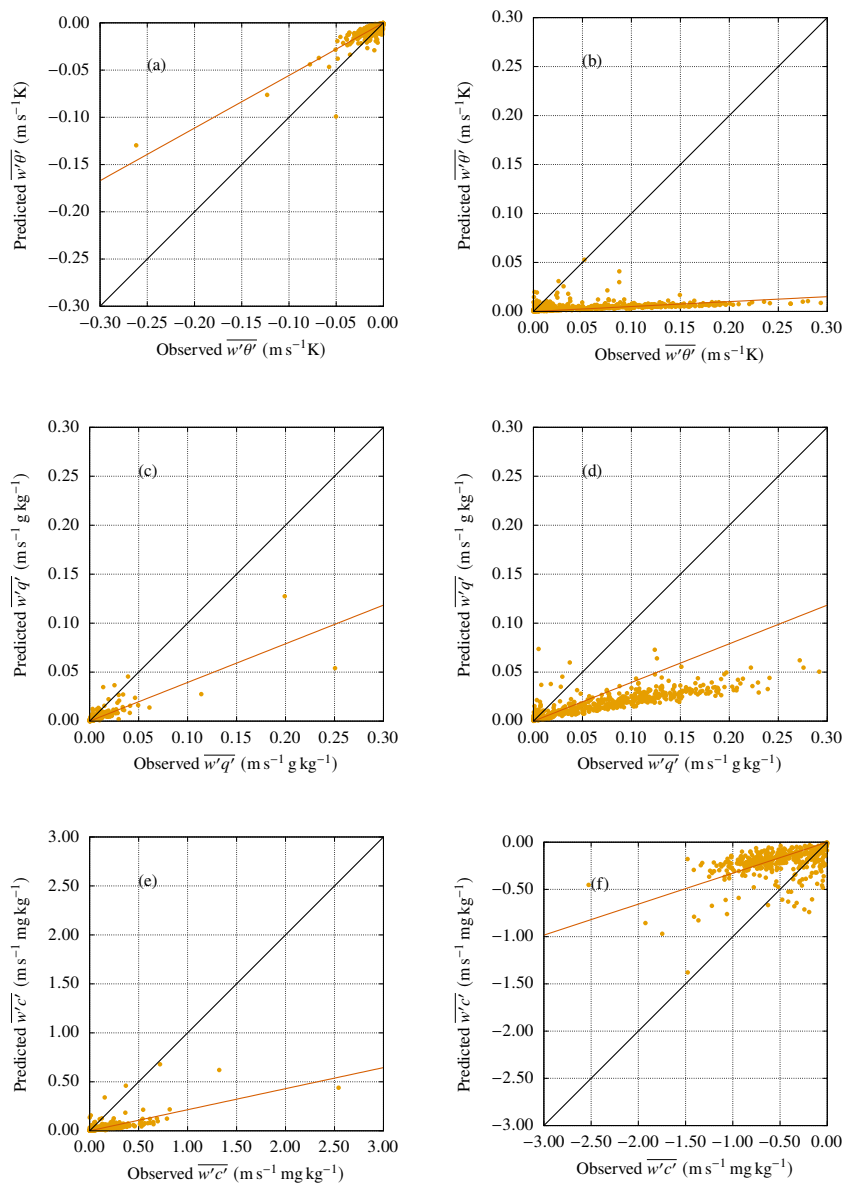


Fig. 5 Observed \times predicted kinematic fluxes $\overline{w's'}$ by the variance method, $s = \theta$ (a,b), $s = q$ (c,d) and $s = c$ (e,f) for stable (a,c,e) and unstable (b,d,f) conditions. The vermilion line is a least-squares fit through the origin, and the black line is $y = x$.

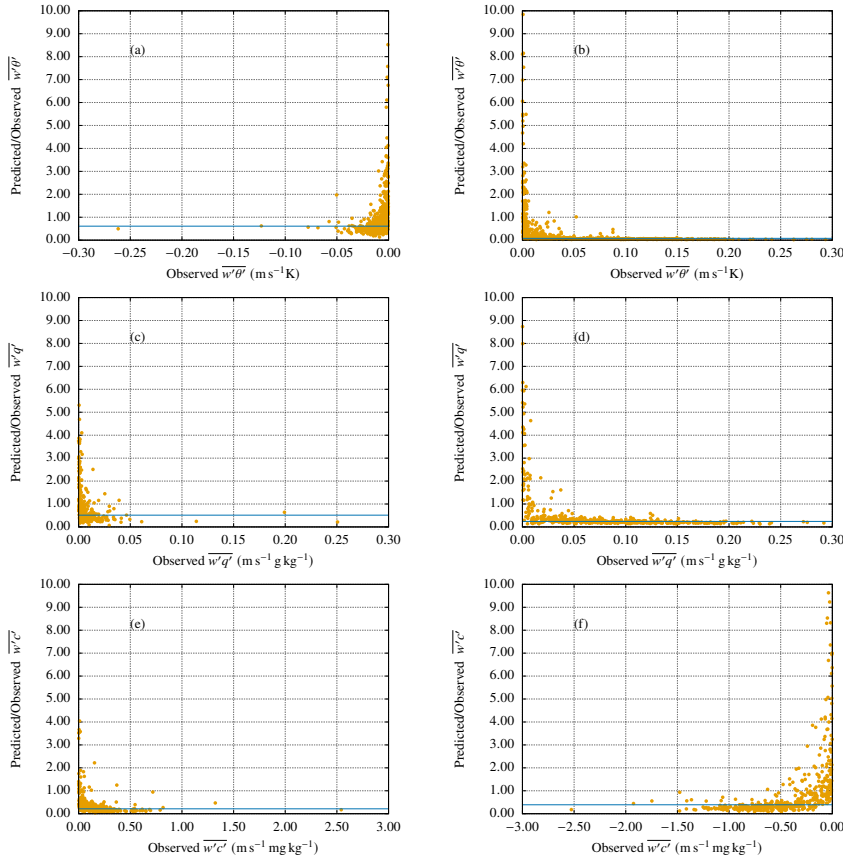


Fig. 6 Observed ratios of predicted to observed kinematic fluxes $\overline{w's'}$ by the variance method, $s = \theta$ (a,b), $s = q$ (c,d) and $s = c$ (e,f) versus the observed fluxes, for stable (a,c,e) and unstable (b,d,f) conditions. The blue line is the median.

339 5.2 Flux estimates from REA-S

340 We applied REA-S for all 3 scalars using the median β_s for each scalar and for
 341 each stability range (stable, unstable) to estimate the fluxes. β_s estimation and
 342 flux performance used the same dataset, since as mentioned earlier the intent
 343 is only to assess the relative potential of the method. The median values of the
 344 obtained β_s s are listed in Table 6. The values of β_s are remarkably close under
 345 each stability regime. They are also clearly different in stable (mean of 0.6049)
 346 and unstable (mean of 0.5564) conditions. While analyzing the REA method
 347 at the same site with a different dataset, Zahn et al. (2016b) obtained similar
 348 values for β_s under unstable conditions, namely a mean of 0.5287 between the
 349 medians of β_θ , β_q and β_c at 39.4 m and 0.5847 at 81.6 m. Thus, it appears

Table 6 Median β_s , for $s = \theta, q, c$, under stable and unstable conditions.

Scalar	Stable	Unstable
θ	0.6090	0.5478
q	0.6036	0.5632
c	0.6021	0.5582
mean	0.6049	0.5564

350 that β_s increases slightly with height in the RSL over the canopy in unstable
 351 conditions.

352 Figure 7 shows the predicted *versus* observed fluxes thus obtained: for each
 353 scalar, we predicted the flux with the corresponding median β_s in Table 6 .
 354 The performance is very good, showing an excellent agreement. Note that the
 355 small variability of β_s among all scalars for the same stability conditions gives
 356 confidence on the applicability of the method, without calibration, at least for
 357 the ATTO site — but bear in mind the β_s dependency on height. The relative
 358 errors of REA-S can be better discerned in Figure 8. The scatter of the small
 359 magnitude fluxes is now much smaller than in Figure 6 for the variance method,
 360 but it is still present, and also likely due, at least in part, to the inherently
 361 more difficult RSL conditions. The scatter is larger for stable than for unstable
 362 conditions. Together, Figures 7 and 8 reconcile the previous results of Zahn
 363 et al. (2016b) and Zahn et al. (2023): plotted on an $x \times y$ graph, the REA shows
 364 excellent performance, but this kind of plot hides the still large variability of
 365 the computed β_s s when plotted (for example) against ζ . Therefore, while the
 366 REA method is probably good enough for mean flux estimates over (say) many
 367 days, one must be cautious when the small-magnitude fluxes are of importance
 368 (say, for specific biophysical processes, etc.).

369 The errors of REA-S are quantified in Table 7. They are much smaller
 370 than those from the variance method (see Table 5), confirming in general the
 371 findings of Zahn et al. (2023), but now for an Amazonian RSL. Note that by es-
 372 timating β_s as the median value, BIAS is virtually eliminated; NMAE remains
 373 below 10% for unstable conditions, and below $\sim 15\%$ for stable conditions.

374 5.3 Flux estimates from REA-T

375 We applied REA-T for q and c with simultaneous measurement of β_θ , assuming
 376 $\beta_{q,c} = \beta_\theta$, and then estimating $\overline{w'q'}$ and $\overline{w'c'}$, for each stability regime (stable,
 377 unstable). This mimics the simultaneous measurement of sonic temperature,
 378 and dispenses with any *a priori* estimate of β_s , but has a built-in assumption of
 379 θ - s scalar similarity. Figure 9 shows the predicted versus observed fluxes thus
 380 obtained. The performance again is very good. The relative errors of REA-T
 381 can be discerned in Figure 10. Figures 9 and 10 look very similar to Figures
 382 7 and 8, showing that both REA-S and REA-T produce reasonably good
 383 results. The same observations about the large scatter of the predicted fluxes
 384 when their magnitude is small apply. The performance statistics in Table 8

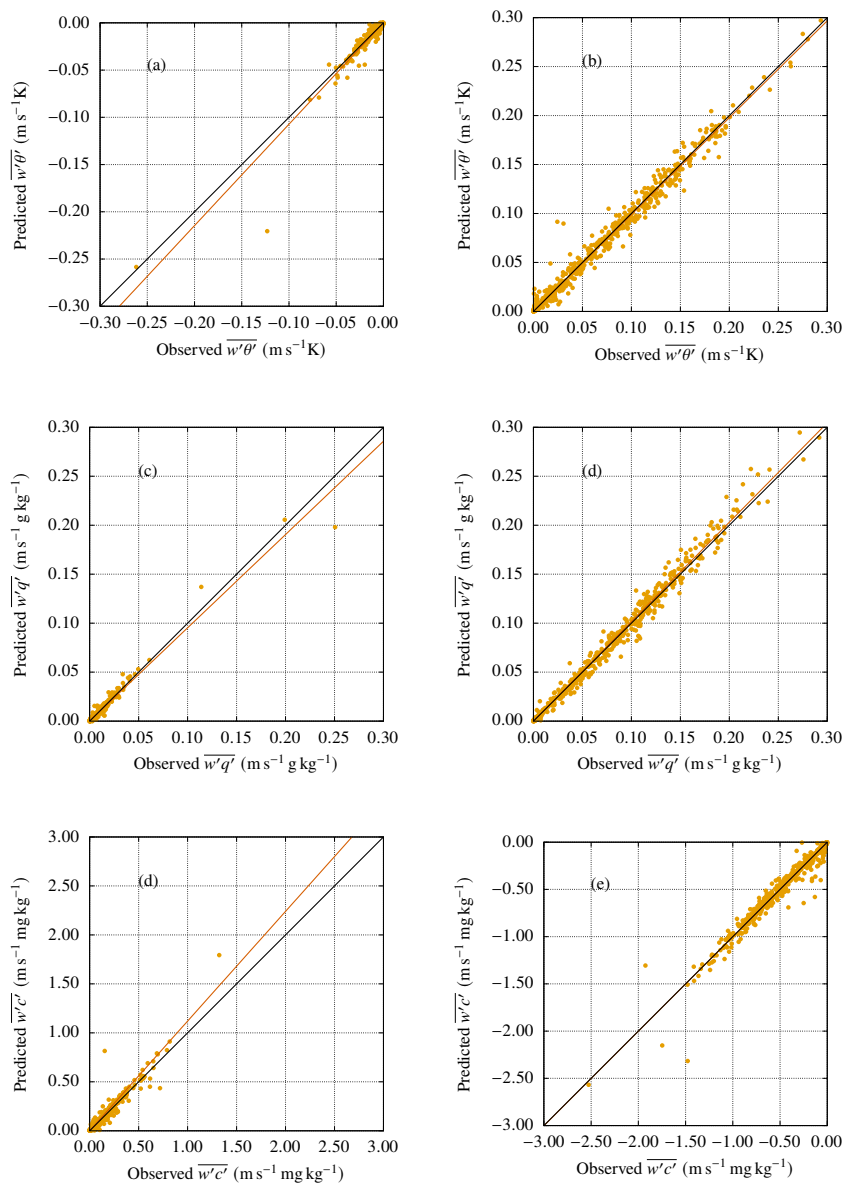


Fig. 7 Observed \times predicted kinematic fluxes $\overline{w's'}$ by means of the REA-S method, $s = \theta$ (a,b), $s = q$ (c,d) and $s = c$ (e,f) for stable (a,c,e) and unstable (b,d,f) conditions. The vermilion line is a least-squares fit through the origin, and the black line is $y = x$.

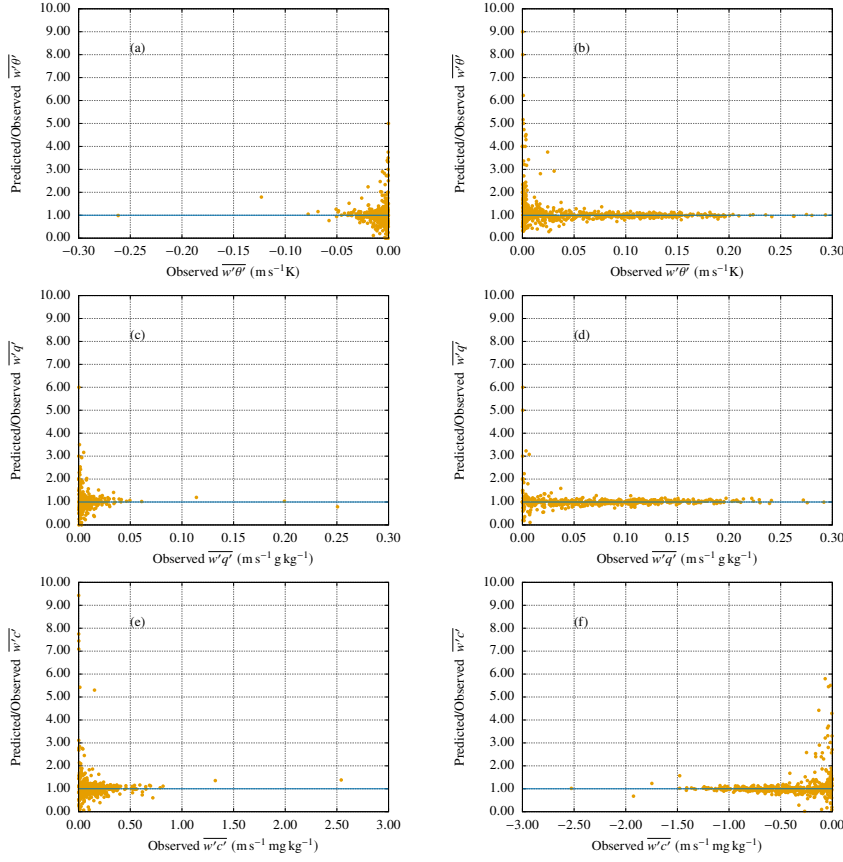


Fig. 8 Observed ratios of predicted to observed kinematic fluxes $\overline{w's'}$ by means of the REA-S method, $s = \theta$ (a,b), $s = q$ (c,d) and $s = c$ (e,f) versus the observed fluxes, for stable (a,c,e) and unstable (b,d,f) conditions. The blue line is the median.

Table 7 Performance statistics for the kinematic fluxes $\overline{w'\theta'}$ ($\text{m s}^{-1}\text{K}$), $\overline{w'q'}$ ($\text{m s}^{-1}\text{g kg}^{-1}$), $\overline{w'c'}$ ($\text{m s}^{-1}\text{mg kg}^{-1}$), estimated by REA-S. BIAS, MAE and RMSE are given in the same corresponding units.

Variable	r	C_d	BIAS	NBIAS	MAE	NMAE	RMSE	NRMSE	d_r
Stable conditions									
$\overline{w'\theta'}$	0.9615	0.8922	-0.0002	-0.0220	0.0016	0.1599	0.0049	0.4817	0.8920
$\overline{w'q'}$	0.9820	0.9637	0.0001	0.0109	0.0013	0.1567	0.0035	0.4302	0.9163
$\overline{w'c'}$	0.9673	0.8736	0.0055	0.0346	0.0247	0.1561	0.0701	0.4429	0.8992
Unstable conditions									
$\overline{w'\theta'}$	0.9926	0.9853	-0.0002	-0.0035	0.0045	0.0742	0.0074	0.1228	0.9565
$\overline{w'q'}$	0.9933	0.9849	0.0006	0.0080	0.0050	0.0628	0.0075	0.0931	0.9500
$\overline{w'c'}$	0.9769	0.9530	-0.0037	-0.0079	0.0422	0.0903	0.0799	0.1710	0.9302

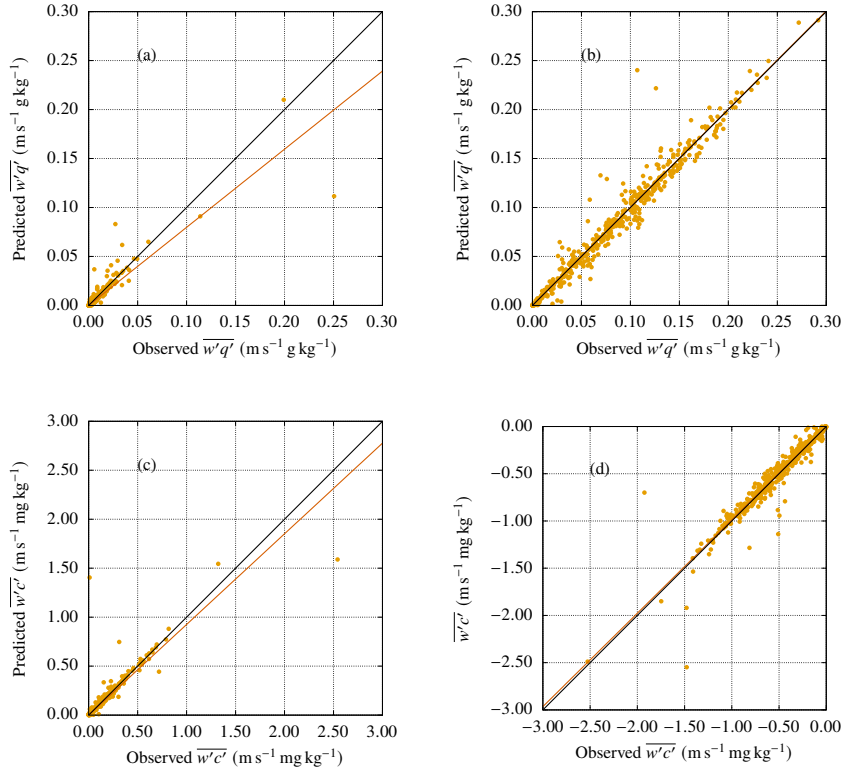


Fig. 9 Observed \times predicted kinematic fluxes $\overline{w's'}$ by means of the REA-T method, $s = q$ (a,b) and $s = c$ (c,d) for stable (a,c) and unstable (b,d) conditions. The vermilion line is a least-squares fit through the origin, and the black line is $y = x$.

385 are somewhat worse than their counterparts in Table 7, but by a small margin
 386 only. Therefore, we deem REA-T as capable as REA-S with the additional
 387 advantage that no *a priori* estimate of β_s is necessary.

388 5.4 Long-term hourly predictive ability of REA

389 Figure 11 shows the hourly means for the whole dataset, for both $s = q$ and $s =$
 390 c , for REA-S (a,c) and REA-T (b,d) against eddy covariance measurements.
 391 The performance of REA-S for $s = \theta$ is very similar to that exhibited for q
 392 and c and is not shown while REA-T for temperature, obviously, makes no
 393 sense. As it can be seen, the REA method's (both versions) ability to capture
 394 the daily cycle and its dispersion around the hourly means is very similar to
 395 the eddy covariance measurements themselves. For the purpose of quantifying

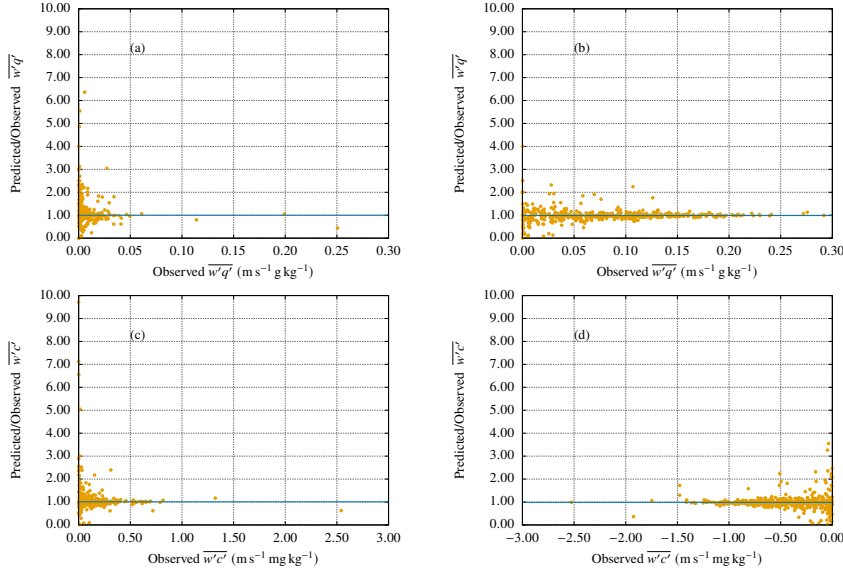


Fig. 10 Observed ratios of predicted to observed kinematic fluxes $\overline{w's'}$ by means of the REA-T method, $s = q$ (a,b) and $s = c$ (c,d) versus the observed fluxes, for stable (a,c) and unstable (b,d) conditions. The blue line is the median.

Table 8 Performance statistics for the kinematic fluxes $\overline{w'q'}$ ($\text{m s}^{-1} \text{g kg}^{-1}$), $\overline{w'c'}$ ($\text{m s}^{-1} \text{mg kg}^{-1}$), estimated by REA-T. BIAS, MAE and RMSE are given in the same corresponding units.

Variable	r	C_d	BIAS	NBIAS	MAE	NMAE	RMSE	NRMSE	d_r
Stable conditions									
$\overline{w'q'}$	0.8948	0.7982	0.0000	0.0045	0.0018	0.2209	0.0084	1.0122	0.8823
$\overline{w'c'}$	0.8949	0.7961	0.0044	0.0276	0.0186	0.1171	0.0893	0.5612	0.9243
Unstable conditions									
$\overline{w'q'}$	0.9789	0.9547	0.0002	0.0022	0.0069	0.0840	0.0128	0.1555	0.9304
$\overline{w'c'}$	0.9617	0.9208	0.0047	0.0098	0.0458	0.0962	0.1036	0.2176	0.9239

396 mass exchanges between the canopy and the atmosphere at the ATTO site
397 (and very likely many other similar forested regions), therefore, our results
398 validate the use of REA as a valuable alternative when fast-response scalar
399 sensors are not available. The one caveat is whether these results also apply
400 for *trace* gases such as CH_4 or isoprene since, if their fluxes are all very small,
401 they might fall in the high scatter region of Figures 8 and 10. In all fairness,
402 the good performance of the REA method over forests is not reported here for
403 the first time; it can be found in Bowling et al. (1999) for water vapor and CO_2
404 fluxes (*c.f.* their Figs 5a, b, c, d). At the same they also show that the scatter

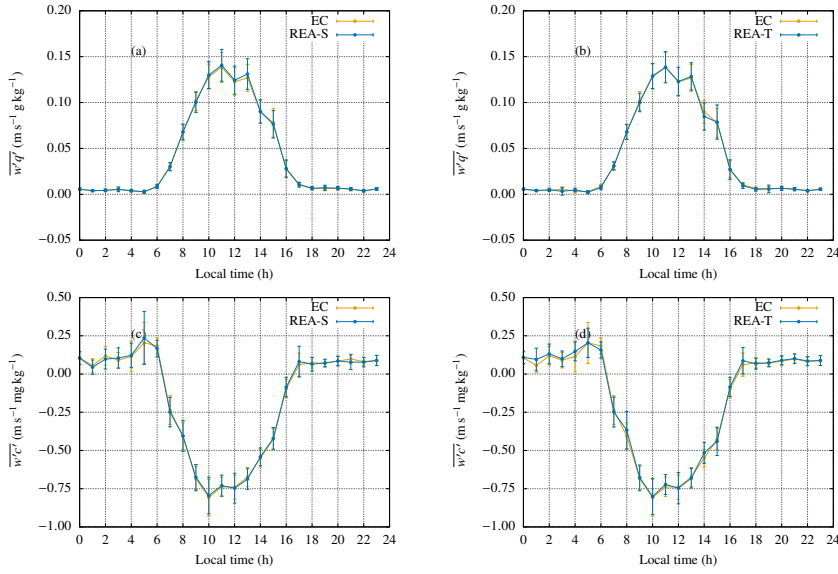


Fig. 11 Hourly means of EC, REA-S and REA-T fluxes at the ATTO site. The bars indicate 1 standard deviation around the means: (a) EC \times REA-S, $s = q$; (b) EC \times REA-T, $s = q$; (c) EC \times REA-S, $s = c$; (d) EC \times REA-T, $s = c$.

405 of the REA method in comparison to eddy covariance is considerably larger for
 406 isoprene flux (*c.f.* their Figs 5e,f) — although this may also be a consequence of
 407 the precision of their isoprene measurements. Clearly, the subject of the ability
 408 of the REA method to produce consistently good results for trace gases will
 409 require further study.

410 6 Discussion and Conclusions

411 The relatively large scatter found for β_s by Zahn et al. (2016b) at the same
 412 site (ATTO) as the present study’s might suggest that the REA method is
 413 not applicable in the RSL of ATTO. However, the recent finding of Zahn
 414 et al. (2023) that the REA can yield rather good results in comparison to EC
 415 measurements even when the scalar in question (in their case, mostly CO₂)
 416 does not conform to MOST, has prompted us to re-visit the issue with ATTO
 417 data. The present work actually reconciles both findings. The β_s scatter *is*
 418 large in the RSL, as can be seen (indirectly) in Figures 8 and 10. On the other
 419 hand, this affects mostly the small-magnitude fluxes. Zahn et al. (2023) showed
 420 very clearly that when any scalar “fails” MOST this is basically caused by
 421 relatively large (in their case) transport and storage terms: at the ATTO site,
 422 other causes such as horizontal and vertical advection might also be playing a
 423 role, on account of the underlying topography (see Chamecki et al. 2020). In

all likelihood, the failure is associated with the small-magnitude fluxes because then the corresponding gradient production term in the scalar semivariance budget is also *relatively* small and the other terms are causing the breakdown of MOST. The term “relatively” is key here, since (again, very likely) the gradient production ultimately is small with respect to the scalar dissipation term. This however, falls outside our present scope and will need to be addressed in future research studies.

Large-magnitude fluxes that occur in the middle of the day, on the other hand, are (again in all likelihood, pending a detailed analysis of the scalar semivariance budgets) associated with a large gradient production term. In this case the β_s s approach the approximately constant values around 0.6 found elsewhere in the literature when measurements were made in the ISL. This is exactly what Zahn et al. (2016b) found for small zenith angles, which naturally occur in the middle of the day, although an explanation based on the scalar semivariance budget was not offered then. These large-magnitude fluxes weigh more heavily in most performance statistics or visual analyses, which tend to hide the large scatter of the small-magnitude fluxes. Moreover, when hourly averages of all data were taken, in Figure 11, the REA method showed considerable ability in reproducing the daily cycle of the EC measurements for the dry season. This lends confidence in the ability of the REA method, despite the shortcomings of RSL-measurements related to the small-magnitude fluxes, of producing reliable estimates of the canopy-atmosphere mass exchanges over timescales larger than (say) several days. In particular, REA-T seems to be a better choice than REA-S since, in spite of slightly larger overall errors, it dispenses with *a priori* assumptions on the value of β_s .

However, to really settle the matter, further research needs to be done:

1. A better understanding of the interplay between the scalar semivariance budget and REA needs to be obtained. For this purpose, a budget as detailed as possible is needed in conjunction with the behavior of β_s under various situations, *viz.* when the gradient production term is large, and when the transport term is large or more generally when a large imbalance between gradient production and dissipation is present.
2. Unfortunately, a criterion for identifying such imbalance that dispenses with EC measurements is lacking; such a criterion would be highly useful for practical quality control of REA measurements. The scalar flux number proposed by Cancelli et al. (2012) might be a useful starting point for this purpose.
3. Scalar variance budgets involving trace gases measured by EC and simultaneous assessment of the REA for these gases are also needed. The present study considered scalars associated with intuitively large fluxes of heat, H₂O and CO₂. A possibility remains that for trace gases the gradient production term is never able to balance dissipation alone. If this happens, then, the REA method is bound to become much more uncertain.

Acknowledgements

This study is part of the Amazon Tall Tower Observatory (ATTO), funded by the German Federal Ministry of Education and Research (BMBF, contracts 01LB1001A and 01LK1602A), the Brazilian Ministry of Science, Technology and Innovation (MCTI/FINEP, contract 01.11.01248.00) and the Max Planck Society (MPG). ATTO is also supported by the Fundação de Amparo à Pesquisa do Estado do Amazonas (FAPEAM), Fundação de Amparo à Pesquisa do Estado de São Paulo (FAPESP), Universidade do Estado do Amazonas (UEA), Instituto Nacional de Pesquisas Amazônia (INPA), Programa de Grande Escala da Biosfera-Atmosfera na Amazônia (LBA) and the SDS/CEUC/RDS-Uatumã. Nelson Luís Dias gratefully acknowledges CNPq's (Brazil's National Research Council) Research Scholarship 305903/2021-7. Cléo Quaresma Dias-Júnior gratefully acknowledges CNPq's (Brazil's National Research Council) Research Scholarship 307530/2022-1.

References

- Andreae, M.O., Acevedo, O.C., Araújo, A., Artaxo, P., Barbosa, C.G.G., Barbosa, H.M.J., Brito, J., Carbone, S., Chi, X., Cintra, B.B.L., da Silva, N.F., Dias, N.L., Dias-Júnior, C.Q., Ditas, F., Ditz, R., Godoi, A.F.L., Godoi, R.H.M., Heimann, M., Hoffmann, T., Kesselmeier, J., Könemann, T., Krüger, M.L., Lavric, J.V., Manzi, A.O., Lopes, A.P., Martins, D.L., Mikhailov, E.F., Moran-Zuloaga, D., Nelson, B.W., Nölscher, A.C., Santos Nogueira, D., Piedade, M.T.F., Pöhlker, C., Pöschl, U., Quesada, C.A., Rizzo, L.V., Ro, C.U., Ruckteschler, N., Sá, L.D.A., de Oliveira Sá, M., Sales, C.B., dos Santos, R.M.N., Saturno, J., Schöngart, J., Sörgel, M., de Souza, C.M., de Souza, R.A.F., Su, H., Targhetta, N., Tóta, J., Trebs, I., Trumbore, S., van Eijck, A., Walter, D., Wang, Z., Weber, B., Williams, J., Winderlich, J., Wittmann, F., Wolff, S., Yáñez-Serrano, A.M., 2015. The amazon tall tower observatory (ATTO): overview of pilot measurements on ecosystem ecology, meteorology, trace gases, and aerosols. *Atmos Chem Phys* 15, 10723–10776. doi:10.5194/acp-15-10723-2015.
- Baker, J., Norman, J., Bland, W., 1992. Field-scale application of flux measurement by conditional sampling. *Agr Forest Meteorol* 62, 31–52. doi:10.1016/0168-1923(92)90004-N.
- Bowling, D., Delany, A., Turnipseed, A., Baldocchi, D., Monson, R., 1999. Modification of the relaxed eddy accumulation technique to maximize measured scalar mixing ratio differences in updrafts and downdrafts. *Journal of Geophysical Research: Atmospheres* 104, 9121–9133. doi:10.1029/1999JD900013.
- Bowling, D.R., Turnipseed, A.A., Delany, A., Baldocchi, D.D., Greenberg, J.P., Monson, R., 1998. The use of relaxed eddy accumulation to measure biosphere-atmosphere exchange of isoprene and other biological trace gases. *Oecologia* 116, 306–315. doi:10.1007/s004420050592.
- Businger, J.A., Oncley, S.P., 1990. Flux measurement with conditional sampling. *J Atmos Oceanic Technol* 7, 349–352. doi:10.1175/1520-0426(1990)007<0349:FMWCS>2.0.CO;2.
- Cancelli, D.M., Dias, N.L., Chamecki, M., 2012. Dimensionless criteria for the production-dissipation equilibrium of scalar fluctuations and their implications for scalar similarity. *Water Resour Res* 48, W10522. doi:10.1029/2012WR012127.
- Chamecki, M., Freire, L.S., Dias, N.L., Chen, B., Dias-Junior, C.Q., Toledo Machado, L.A., Sörgel, M., Tsokankunku, A., Araújo, A., 2020. Effects of vegetation and topography on the boundary layer structure above the amazon forest. *J Atmos Sci* 77, 2941–2957. doi:10.1175/JAS-D-20-0063.1.

- 516 Chor, T.L., Dias, N.L., Araújo, A., Wolff, S., Zahn, E., Manzi, A., Trebs, I., Sá, M.O.,
517 Teixeira, P.R., Sörgel, M., 2017. Flux-variance and flux-gradient relationships in the
518 roughness sublayer over the Amazon forest. *Agr Forest Meteorol* 239, 213–222.
519 doi:10.1016/j.agrformet.2017.03.009.
- 520 Desjardins, R.L., 1972. A study of carbon-dioxide and sensible heat fluxes using the eddy
521 correlation technique. Ph.D. thesis. Cornell University.
- 522 Desjardins, R.L., 1977. Description and evaluation of a sensible heat flux detector.
523 *Boundary-Layer Meteorol* 11, 147–154. doi:10.1007/BF02166801.
- 524 Dias, N.L., 2013. Research on atmospheric turbulence by Wilfried Brutsaert and collabora-
525 tors. *Water Resour Res* 49, 7169–7184. doi:10.1002/wrcr.20461.
- 526 Dias, N.L., Brutsaert, W., 1996. Similarity of scalars under stable conditions. *Boundary-*
527 *Layer Meteorol* 80, 355–373. doi:10.1007/BF00119423.
- 528 Dias, N.L., Hong, J., Leclerc, M., Black, Nescic, Z., Krishnan, P., 2009. A simple method
529 of estimating scalar fluxes over forests. *Boundary-Layer Meteorol* 132, 401–414.
530 doi:10.1007/s10546-009-9408-0.
- 531 Dias-Júnior, C.Q., Dias, N.L., dos Santos, R.M.N., Sörgel, M., Araújo, A., Tsokankunku,
532 A., Ditas, F., de Santana, R.A., von Randow, C., Sá, M., et al., 2019. Is there a clas-
533 sical inertial sublayer over the amazon forest? *Geophys Res Lett* 46, 5614–5622.
534 doi:10.1029/2019GL083237.
- 535 Edson, J.B., Fairall, C.W., Bariteau, L., Zappa, C.J., Cifuentes-Lorenzen, A., McGillis,
536 W.R., Pezoa, S., Hare, J.E., Helmig, D., 2011. Direct covariance measurement of CO₂
537 gas transfer velocity during the 2008 southern ocean gas exchange experiment: Wind
538 speed dependency. *J Geophys Res-Oceans* 116, C00F10. doi:10.1029/2011JC007022.
- 539 Fuentes, J.D., Chamecki, M., dos Santos, R.M.N., von Randow, C., Stoy, P.C., Katul,
540 G., Fitzjarrald, D., Manzi, A., Gerken, T., Trowbridge, A., Freire, L.S., Ruiz-
541 Plancarte, J., Maia, J.M.F., Tóta, J., Dias, N.L., Fisch, G., Schumacher, C., Acevedo,
542 O., Mercer, J.R., 2016. Linking meteorology, turbulence, and air chemistry in
543 the amazon rainforest. *Bull Amer Meteorol Soc* 97, 2329–2342. URL:
544 <http://dx.doi.org/10.1175/BAMS-D-15-00152.1>, doi:10.1175/BAMS-D-15-00152.1.
- 545 Hill, R.J., 1989. Implications of Monin-Obukhov similarity theory for scalar quantities.
546 *J Atmos Sci* 46, 2236–2244. doi:10.1175/1520-0469(1989)046<2236:IOMSTF>2.0.CO;2.
- 547 Katul, G., Peltola, O., Grönholm, T., Launiainen, S., Mammarella, I., Vesala, T., 2018. Ejec-
548 tive and sweeping motions above a peatland and their role in relaxed-eddy-accumulation
549 measurements and turbulent transport modelling. *Boundary-Layer Meteorol* 169, 163–
550 184. doi:10.1007/s10546-018-0372-4.
- 551 McMillen, R.T., 1988. An eddy correlation technique with extended applicability to non-
552 simple terrain. *Boundary-Layer Meteorol* 43, 231–245. doi:10.1007/BF00128405.
- 553 Mochizuki, T., Tani, A., Takahashi, Y., Saigusa, N., Ueyama, M., 2014. Long-term measure-
554 ment of terpenoid flux above a larch kaempferi forest using a relaxed eddy accumulation
555 method. *Atmos Environ* 83, 53–61. doi:10.1016/j.atmosenv.2013.10.054.
- 556 Mortarini, L., Katul, G.G., Cava, D., Dias-Junior, C.Q., Dias, N.L., Manzi, A., Sorgel, M.,
557 Araújo, A., Chamecki, M., 2023. Adjustments to the law of the wall above an amazon
558 forest explained by a spectral link. *Phys Fluids* 35. doi:10.1063/5.0135697.
- 559 Ren, X., Sanders, J., Rajendran, A., Weber, R., Goldstein, A., Pusede, S., Browne, E., Min,
560 K.E., Cohen, R., 2011. A relaxed eddy accumulation system for measuring vertical fluxes
561 of nitrous acid. *Atmos Meas Tech* 4, 2093–2103. doi:10.5194/amt-4-2093-2011.
- 562 Rhew, R.C., Deventer, M.J., Turnipseed, A.A., Warneke, C., Ortega, J., Shen, S., Martinez,
563 L., Koss, A., Lerner, B.M., Gilman, J.B., et al., 2017. Ethene, propene, butene and
564 isoprene emissions from a ponderosa pine forest measured by relaxed eddy accumulation.
565 *Atmos Chem Phys* 17, 13417–13438. doi:10.5194/acp-17-13417-2017.
- 566 Santana, R.A., Dias-Júnior, C.Q., da Silva, J.T., Fuentes, J.D., do Vale, R.S., Alves, E.G.,
567 dos Santos, R.M.N., Manzi, A.O., 2018. Air turbulence characteristics at multiple
568 sites in and above the amazon rainforest canopy. *Agr Forest Meteorol* 260, 41–54.
569 doi:10.1016/j.agrformet.2018.05.027.
- 570 Sarkar, C., Turnipseed, A., Shertz, S., Karl, T., Potosnak, M., Bai, J., Serça, D., Bonal, D.,
571 Burban, B., Lopes, P.R., et al., 2020. A portable, low-cost relaxed eddy accumulation
572 (REA) system for quantifying ecosystem-level fluxes of volatile organics. *Atmos Envi-*
573 *ron* 242, 117764. doi:10.1016/j.atmosenv.2020.117764.

- 574 Webb, E.K., Pearman, G.I., Leuning, R., 1980. Correction of flux measurements for density
575 effects due to heat and water vapor transfer. *Q J R Meteorol Soc* 106, 85–100.
576 doi:10.1002/qj.49710644707.
- 577 Willmott, C.J., Robeson, S.M., Matsuura, K., 2012. A refined index of model performance.
578 *Int J Climatol* 32, 2088–2094. doi:10.1002/joc.2419.
- 579 Zahn, E., Bou-Zeid, E., Dias, N.L., 2023. Relaxed eddy accumulation outperforms Monin-
580 Obukhov flux models under non-ideal conditions. *Geophys Res Lett* 50, e2023GL103099.
581 doi:10.1029/2023GL103099.
- 582 Zahn, E., Chor, T.L., Dias, N.L., 2016a. A simple methodology for quality control of microm-
583 eteorological datasets. *Am J Environ Eng* 6, 135–142. doi:10.5923/s.ajee.201601.20.
- 584 Zahn, E., Dias, N.L., Araújo, A., Sá, L.D.A., Sörgel, M., Trebs, I., Wolff, S., Manzi, A.,
585 2016b. Scalar turbulent behavior in the roughness sublayer of an amazonian forest.
586 *Atmos Chem Phys* 16, 11349–11366. doi:10.5194/acp-16-11349-2016.
- 587 Zhu, T., Pattey, E., Desjardins, R., 2000. Relaxed eddy-accumulation technique for mea-
588 suring ammonia volatilization. *Environ Sci Technol* 34, 199–203. doi:10.1021/es980928f.